PHYSICAL REVIEW C **81**, 011901(R) (2010)

Indication of divergent baryon-number susceptibility in QCD matter

N. G. Antoniou,* F. K. Diakonos,† and A. S. Kapoyannis‡
Department of Physics, University of Athens, GR-15771 Athens, Greece
(Received 11 July 2008; revised manuscript received 6 November 2009; published 4 January 2010)

The baryon-number density formed in relativistic nuclear collisions versus the chemical potential of the freeze-out states is systematically studied on the basis of existing measurements. A remarkable power-law behavior of the baryon-number susceptibility is found at the CERN Super Proton Synchrotron, consistent with the existence of a QCD critical point at $\mu_{B,c} \simeq 222$ MeV, $T_c \simeq 155$ MeV. The equation of state in different asymptotic regimes of the critical region is also examined and confronted with freeze-out states in these experiments.

DOI: 10.1103/PhysRevC.81.011901 PACS number(s): 25.75.Nq, 05.70.Ce, 12.38.Mh, 21.65.Qr

Baryons produced in collisions of nuclei at relativistic energies play an important role in the identification of critical states in strongly interacting matter [1,2]. The baryon-number density $n_B(\vec{x})$ is an appropriate order parameter of the critical system, equivalent to the chiral field $\sigma(\vec{x})$ because they both incorporate in their behavior the universal power laws and the related exponents of the QCD critical point [1]. A complete set of observables associated either with the baryon-number density or the σ field may form together with the corresponding measurements in experiments with nuclei the basic ingredients and tools for the construction of an observational theory of critical QCD matter [2,3]. Power-law fluctuations in the isoscalar component of $\pi^+\pi^-$ pairs near the two-pion threshold or in the net-baryon system produced at midrapidity are examples of such observables [2,3].

In this article we search for a singular behavior of baryon-number susceptibility χ_B exploiting the existing measurements of baryochemical potential in a series of freeze-out states ranging from CERN Super Proton Synchrotron (SPS) to Relativistic Heavy Ion Collider (RHIC) energies. The guidelines in this investigation come from the universal properties of the equation of state for 3D Ising systems, which specify the universality class of the QCD critical point [4]. The observables in this treatment are (a) the baryon number density n_B, properly averaged in a space-time region occupied by the system, and (b) the baryochemical potential μ_B and the temperature T of the corresponding freeze-out state. The behavior near the critical point is described by the order parameter $\rho_B = n_B - n_{B,c}$ and the conjugate ordering field $m = \frac{\mu_B - \mu_{B,c}}{\mu_{B,c}}$. With these variables the equation of state near the critical point is written as follows:

$$B_c^{\delta}|m| = |\rho_B|^{\delta} F\left(B^{1/\beta}\frac{t}{|\rho_B|^{1/\beta}}, \frac{R}{\xi}\right); \quad t = \frac{T - T_c}{T_c}, \tag{1a}$$

where R is the linear size of the system after the collision of nuclei and ξ the corresponding correlation length. Equation (1a) is based on the conjecture of finite-size scaling [5] and in the limit of infinite volume ($R \to \infty$) one obtains the universal form [6]:

$$B_c^{\delta}|m| = |\rho_B|^{\delta} f\left(B^{1/\beta}\frac{t}{|\rho_B|^{1/\beta}}\right). \tag{1b}$$

Obviously, Eq. (1b) is approximately valid also for finite systems under the constraint $R \gg \xi$. In this work we exploit Eq. (1b) in nuclear systems of different sizes assuming that this constraint holds. With this assumption finite-size effects in the equation of state become negligible.

In Eq. (1b) the scaling function $f(x)$ is universal and properly normalized: $f(0) = 1$ and $f(-1) = 0$ [6]. Moreover, the function $f(x)$ is regular at the point $x = 0$ and follows a power law, $f(x) \sim x^{\gamma}$, for large x [6]. The constants B_c and B in Eq. (1b) are nonuniversal amplitudes and the critical exponents β, γ, and δ are fixed by the 3D Ising-QCD universality class ($\beta \simeq \frac{1}{3}$, $\gamma \simeq \frac{4}{3}$, $\delta \simeq 5$).

In the notation of Ref. [6] the critical equation of state for strongly interacting matter, given by the generic Eq. (1b), is specified as follows [6]:

$$y = f(x); \quad x = \frac{B^{1/\beta}t}{|\rho_B|^{1/\beta}}, \quad y = \frac{B_c^{\delta}|m|}{|\rho_B|^{\delta}} \tag{2a}$$

$$f(x) = 1 + \sum_{n=1}^{\infty} f_n^{(0)} x^n \quad (x \simeq 0) \tag{2b}$$

$$f(x) = x^{\gamma} \sum_{n=0}^{\infty} f_n^{\infty} x^{-2n\beta} \quad (x \to \infty). \tag{2c}$$

For 3D Ising systems, the coefficients $(f_n^{(0)}, f_n^{\infty})$ have been evaluated in Ref. [6] for $n \leqslant 5$, using renormalization group techniques. The truncation of the series consisting of Eqs. (2b) and (2c) at the maximal order $n = 5$ leads to a good approximation of $f(x)$ in the limiting regimes ($x \simeq 0$, $x \to \infty$) but also guarantees a smooth transition from one region to the other around the point $x \simeq 1$.

Within the framework of Eqs. (2) one may approach the critical point following distinct paths in the QCD phase diagram: for $t = 0$ one moves along the critical isotherm, $|\rho_B| = B_c|m|^{1/\delta}$, and the baryon-number susceptibility, $\chi_B = \frac{\partial n_B}{\partial \mu_B}$, develops a power-law singularity for $m = 0$, $\chi_B \sim |m|^{-\varepsilon}$, a clear signal of a critical point ($\varepsilon = \frac{\delta - 1}{\delta}$). For $t < 0, m = 0$ the coexistence line, $|\rho_B| = B|t|^{\beta}$, which is a limiting curve of the family (2a) when $m \to 0$ is traced. In the general case ($m \neq 0$),

*nantonio@phys.uoa.gr
†fdiakono@phys.uoa.gr
‡akapog@phys.uoa.gr

Eq. (2a) penetrates the crossover regime for $t > 0$ with a smooth dependence of ρ_B on t. Finally, in the limit $x \to \infty$, the system follows the critical isochor ($\rho_B \to 0$) along which the baryon-number susceptibility obeys the power-law $\chi_B = C_\chi |t|^{-\gamma}$ with the amplitude $C_\chi = \frac{B_c^\delta}{f_0^\infty B^{\gamma/\beta}}$. This landscape of universal power laws, extracted from the exact equation of state, may be confronted with measurements of the observables n_B, μ_B, and T in relativistic nuclear collisions to capture the critical region of strongly interacting matter.

The net-baryon density n_B (fm^{-3}) is fixed, in this treatment, at midrapidity, with the averaging scale $\delta y \simeq 2$ corresponding to a region of approximately constant rapidity distribution. The proper time scale for the freeze-out state is taken $\langle \tau \rangle \simeq 2.5$ fm, on the average, assuming a weak dependence of τ on A. In this description, the density $n_B(0)$ is given in terms of measurable quantities by the simple expression $n_B(0) = \frac{A_{\min}^{-2/3}}{\pi r_0^2 \langle \tau \rangle} (\frac{dN_B}{dy})_0$, where $(\frac{dN_B}{dy})_0$ denotes the baryon number per unit of rapidity in the central region. In this expression, the transverse area of the system is fixed by the standard scale of nuclear sizes $r_0 \simeq 1.2$ fm and the quantity $A_{\min} = \frac{A_w}{2}$ in the case of identical colliding nuclei $A + A$ or $A_{\min} = \min(A, A')$ in the case of nonidentical colliding nuclei $A + A'$ (A_w denotes the number of wounded nucleons).

In Table I we summarize the experiments with nuclei ($A + A'$) and the corresponding measurements of the relevant observables, in a wide range of energies and sizes of the colliding systems. The baryonic densities and the corresponding errors have been calculated using either the formula [7]

$$B - \bar{B} = (2.07 \pm 0.05)(p - \bar{p}) + (1.6 \pm 0.1)(\Lambda - \bar{\Lambda}) \quad (3)$$

or the formula [8]

$$B - \bar{B} = (1 + a)(p - \bar{p}) + 2\frac{1 + b}{1 + 2b}(K^+ - K^-), \quad a = 1.07, \ b = 0.1. \quad (4)$$

In Fig. 1 the freeze-out states in experiments at the SPS and RHIC are located in the diagram $n_B(0)$ versus μ_B. The errors

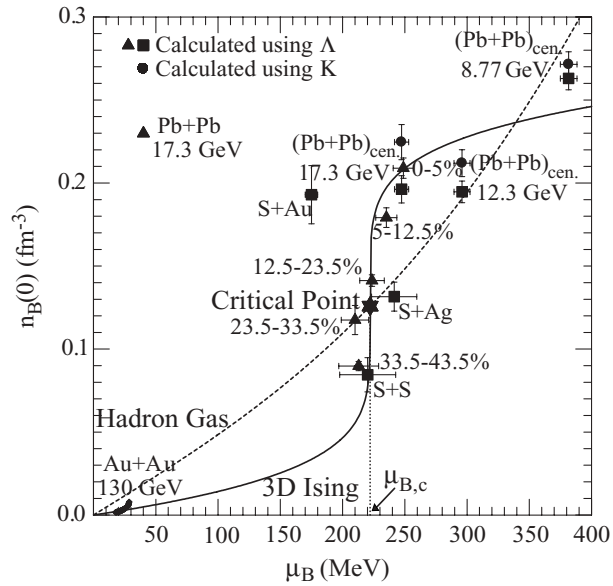

FIG. 1. The baryon number density at midrapidity $n_B(0)$ versus baryochemical potential μ_B is illustrated for a series of freeze-out states, calculated for $\langle \tau \rangle = 2.5$ fm. The solid line represents the best-fit solution in the description of the Pb + Pb ($\sqrt{s} = 17.3$ GeV) central and peripheral data with the critical isotherm ($T \simeq 155$ MeV) equation of state. The dashed line corresponds to the HG model prediction in the same region calculated for average baryon volume $v_0 = 7.63$ fm^3 [21].

in μ_B (listed in Table I) are taken from the corresponding references. The errors in $n_B(0)$ are due to errors in $A_{\min}$ and $(\frac{dN_B}{dy})_0$. Data used in Figs. 1, 2, and 4 are given in Table II. The experimental points belong to three distinct classes of measurements: (a) central and peripheral Pb + Pb collisions at the SPS (NA49 experiments), (b) central collisions of light nuclei (S) at the SPS (NA35 experiments), and (c) central and peripheral Au + Au collisions at RHIC. In the states of class (a) and in particular for the highest SPS energy ($\sqrt{s} \simeq 17$ GeV), the freeze-out temperature remains practically constant

TABLE I. Measurements of the relevant observables in experiments with nuclei.

$A + A'$	$\sqrt{s}$ (GeV)	A_w	$\left(\frac{dN_B}{dy}\right)_0$	μ_B (MeV)	T (MeV)	Ref.
$(S + S)_{cen.}$	19.4	54 ± 3	8.6 ± 1[a]	220 ± 22	180.5 ± 10.9	[9–11]
$(S + Ag)_{cen.}$	16.3	90 ± 10	15 ± 1[a]	242 ± 18	178.9 ± 8.1	[10,11]
$(S + Au)_{cen.}$	13.5	113	22 ± 2[a]	175 ± 5	165 ± 5	[9,10,12]
$(Pb + Pb)_{cen.}$	8.77	349 ± 5	104.4 ± 2.7[a], 107.8 ± 3.0[b]	381.6 ± 6.7	144.6 ± 2.3	[13,14]
$(Pb + Pb)_{cen.}$	12.3	349 ± 5	77.3 ± 2.6[a], 84.2 ± 3.2[b]	296.0 ± 6.4	151.7 ± 2.9	[13,14]
$(Pb + Pb)_{cen.}$	17.3	362 ± 8	71.0 ± 2.8[a], 81.3 ± 3.6[b]	247.4 ± 5.7	156.1 ± 1.6	[13,14]
$(Pb + Pb)_{0–5\%}$	17.3	361	75.5 ± 2.2[a]	248.9 ± 8.2	157.5 ± 2.2	[13,15]
$(Pb + Pb)_{5–12.5\%}$	17.3	304 ± 10	57.7 ± 1.4[a]	235.2 ± 8.5	150.6 ± 3.2	[13,15]
$(Pb + Pb)_{12.5–23.5\%}$	17.3	226	37.3 ± 0.9[a]	223.7 ± 9.9	156.6 ± 3.7	[13,15]
$(Pb + Pb)_{23.5–33.5\%}$	17.3	158	24.5 ± 1.8[a]	210 ± 11	154.7 ± 4.2	[13,15]
$(Pb + Pb)_{33.5–43.5\%}$	17.3	110	14.7 ± 0.4[a]	213 ± 16	153.2 ± 5.9	[13,15]
$(Au + Au)_{cen.–per.}$	130	381–4.9	(29.2–0.3)[a]	28.6–17.6	165	[16–19]

[a]Calculated using $\Lambda - \bar{\Lambda}$.
[b]Calculated using $K^+ - K^-$.

TABLE II. Data used for the vertical axis values in Figs. 1, 2, and 4. The horizontal axis values are listed in the μ_B column (Figs. 1 and 2) and in the T column (Fig. 4) of Table I.

$A + A'$	$\sqrt{s}$ (GeV)	$n_B(0)$ (fm^{-3})	$\lvert\rho_B(0)\rvert$ (fm^{-3})
$(S + S)_{cen.}$	19.4	0.084 ± 0.010[a]	0.041 ± 0.010[a]
$(S + Ag)_{cen.}$	16.3	0.132 ± 0.009[a]	0.006 ± 0.009[a]
$(S + Au)_{cen.}$	13.5	0.193 ± 0.018[a]	0.067 ± 0.018[a]
$(Pb + Pb)_{cen.}$	8.77	0.271 ± 0.008[b]	
$(Pb + Pb)_{cen.}$	8.77	0.263 ± 0.007[a]	0.137 ± 0.007[a]
$(Pb + Pb)_{cen.}$	12.3	0.212 ± 0.008[b]	
$(Pb + Pb)_{cen.}$	12.3	0.195 ± 0.006[a]	0.069 ± 0.006[a]
$(Pb + Pb)_{cen.}$	17.3	0.225 ± 0.011[b]	0.099 ± 0.011[b]
$(Pb + Pb)_{cen.}$	17.3	0.196 ± 0.008[a]	0.070 ± 0.008[a]
$(Pb + Pb)_{0-5\%}$	17.3	0.209 ± 0.006[a]	0.083 ± 0.006[a]
$(Pb + Pb)_{5-12.5\%}$	17.3	0.179 ± 0.006[a]	0.053 ± 0.006[a]
$(Pb + Pb)_{12.5-23.5\%}$	17.3	0.141 ± 0.003[a]	0.015 ± 0.003[a]
$(Pb + Pb)_{23.5-33.5\%}$	17.3	0.117 ± 0.009[a]	0.008 ± 0.009[a]
$(Pb + Pb)_{33.5-43.5\%}$	17.3	0.090 ± 0.003[a]	0.036 ± 0.003[a]
$(Au + Au)_{cen.-per.}$	130	0.0079–0.0016[a]	0.118–0.124[a]

[a]Calculated using $\Lambda - \bar{\Lambda}$.
[b]Calculated using $K^+ - K^-$.

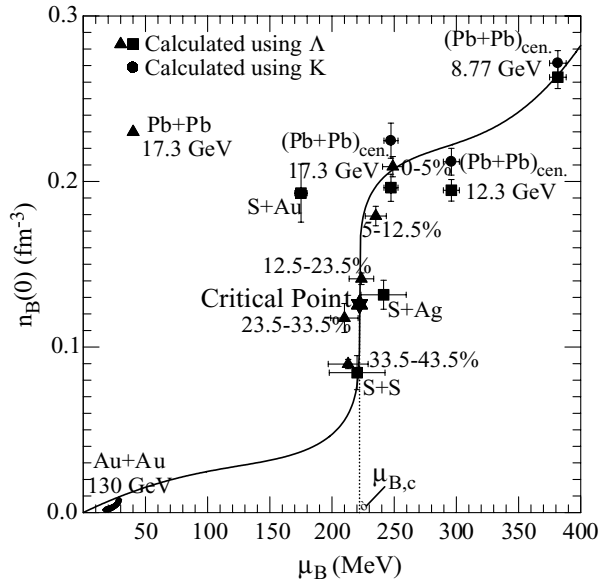

FIG. 2. The same illustration as in Fig. 1. The solid line represents the combination of the two models of Fig. 1 with a Gaussian weight extended to a region of magnitude $\sigma_{\text{Gauss}} \simeq 142$ MeV around the critical baryochemical potential $\mu_{B,c}$.

(Table I) and the actual value measured in these experiments is fixed, on average, at the level $\langle T \rangle \simeq 155$ MeV. As a result, we may assume that the experimental points of class (a) belong to an isotherm which, as shown in Fig. 1, develops a very large derivative $\frac{\partial n_B}{\partial \mu_B}$ near the value $\mu_B \simeq 222$ MeV of the chemical potential. This observation implies that the baryon-number susceptibility of strongly interacting matter may become infinitely large in this region of the phase diagram ($T \simeq 155$ MeV, $\mu_B \simeq 222$ MeV). It is therefore suggestive that the freeze-out states in class (a) form a critical isotherm associated with the 3D Ising-QCD critical point.

To verify quantitatively this hypothesis, starting from the observations made earlier in this article, one must employ the critical equation of state discussed in the first part of this article [Eqs. (1) and (2)], in the case where $t = 0$ (critical isotherm). In other words, one must be able to describe the freeze-out states of class (a) in the diagram of Fig. 1 with the equation of state:

$$\left|n_B(0) - n_{B,c}\right| = B_c \left|\frac{\mu_B - \mu_{B,c}}{\mu_{B,c}}\right|^{\frac{1}{\delta}}. \qquad (5)$$

With the normalization condition $n_B = 0$ for $\mu_B = 0$, the best-fit solution ($\chi^2/\text{dof} \simeq 0.59$) is illustrated in Fig. 1 and corresponds to the actual values of the parameters $n_{B,c} = (0.126^{+0.025}_{-0.007})$ fm^{-3}, $\mu_{B,c} = (222 \pm 14)$ MeV ($B_c \simeq n_{B,c}$) with confidence level (CL) for the errors 95.4%.

The standard description of heavy-ion freeze-out data is given by the statistical hadron gas (HG) model [20,21], which also includes volume corrections to account for the repulsive part of hadron interaction. The HG model explains quite well the trend of the data in the phase diagram; however, this model does not include interactions among hadrons (apart from a repulsive part treated a la Van der Waals) and so cannot accommodate any kind of phase transition or critical point. In the vicinity of the critical point the system should exhibit universal behavior; thus, the system can be better described by an equation of state (EOS) belonging to 3D Ising universality class. The different behavior of the two theories near the critical point is depicted in Fig. 1. The HG model (with volume corrections) isotherm (for the same temperature: $T \simeq 155$ MeV) predicts a smooth behavior in contrast to the 3D Ising model, which leads to divergent susceptibility, consistent with the data in this restricted area. The model that combines the behavior near to, as well as away from, the critical point is a two-component model. It is calculated using the HG model EOS with a properly suited Gaussian weight which switches on the 3D Ising model and switches off the HG model as one approaches the critical point.

In Fig. 2, the two-component description of the baryon-number susceptibility is illustrated with the universal 3D Ising component dominating the nearby region of the critical point. It is of interest to note that as we depart from the critical point, the hadron gas becomes important and dominates the susceptibility with a nonuniversal component for $\mu_B > 400$ MeV.

In summary, we have been able to isolate a class of freeze-out states corresponding to central and peripheral Pb + Pb collisions at $\sqrt{s} \simeq 17$ GeV which form a critical isotherm associated with a QCD critical point at a location in the phase diagram fixed by the values $T_c \simeq 155$ MeV, $\mu_{B,c} \simeq 222$ MeV. The baryon-number susceptibility, $\chi_B \sim |\mu_B - \mu_{B,c}|^{\frac{1-\delta}{\delta}}$, diverges at the critical point according to a universal power law, fixed by the critical exponent δ [Eq. (5)]. In Fig. 3, the singularity of χ_B corresponding to solution (5) is illustrated together with the results of a crude differentiation of nearby experimental points in Fig. 1. The trend is consistent with the derivative of solution (5), in particular if we take into

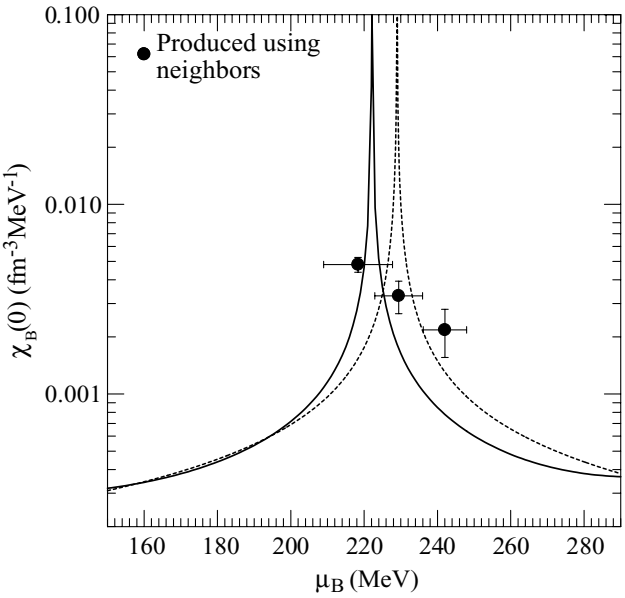

FIG. 3. The baryon-number susceptibility χ_B for $T = T_c$ versus μ_B. The solid line corresponds to the derivative of the best-fit solution shown in Fig. 2. The dashed line corresponds to the 3D Ising case with $n_{B,c} = 1.71$ fm^{-3} and $\mu_{B,c} = 229$ MeV (values within the CL = 95.4% error of the best-fit parameters of Fig. 1). The data points are produced using neighboring differences.

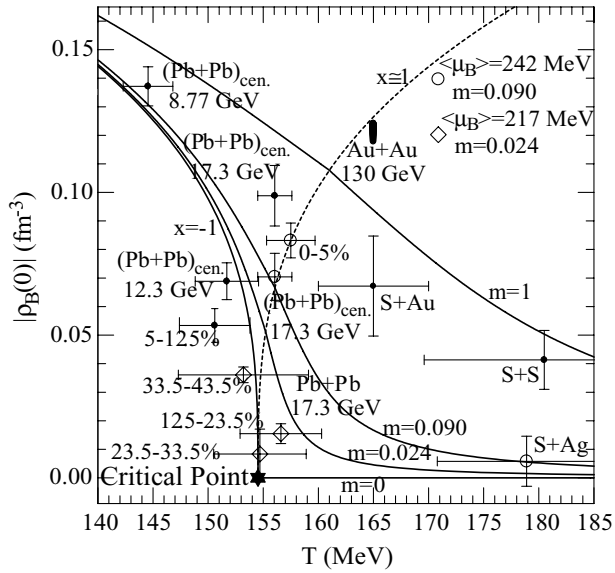

FIG. 4. The equation of state $|\rho_B|$ versus T, for $m = \text{const}$. The curve $m = 0$, $T \leqslant T_c$ corresponds to the coexistence line and for $T \geqslant T_c$ to the critical isochor. The experimental freeze-out states are located within the area spanned by the family of curves of constant m.

account the errors of the fitted parameters. Data used in Fig. 3 are given in Table III.

In this last part of our treatment we attempt to exploit, beyond the critical isotherm, the universal properties of the critical equation of state which are rigorously incorporated in representation (2). To this end, in Fig. 4 we consider the diagram $|\rho_B(0)|$ versus T in which the freeze-out states are properly located together with the critical point found in our approach. With the help of Eqs. (2) we have constructed, in the same figure, the family of curves corresponding to different values of m and representing the critical equation of state in its full capacity (critical surface). To obtain a line of constant m we first give a certain value to $\rho_B(0)$, and so, according to Eq. (2a), y is fixed. Then we solve numerically the equation $x = f(x)$ [Eqs. (2b) and (2c)] to obtain x and finally the temperature T through Eqs. (2a) and (1). Across the family of curves of constant m we have drawn the curve $x \simeq 1$

TABLE III. Data used in Fig. 3. The susceptibility is calculated between neighbors for the $\sqrt{s} = 17.3$ GeV Pb + Pb data for various centralities i, j, $\chi_B(0) = \frac{n_B(0)_j - n_B(0)_i}{\mu_{B,j} - \mu_{B,i}}$. The corresponding baryochemical potential μ_B is calculated as the average of the relevant chemical potentials $\mu_{B,j}$, $\mu_{B,i}$. The errors in $n_B(0)_{i,j}$ and $\mu_{B,i,j}$ are taken from Table II.

i, j (%)	$\chi_B(0)$ (fm^{-3} MeV^{-1})	μ_B (MeV)
0–5, 5–12.5	0.0022 ± 0.0006	242.1 ± 5.9
5–12.5, 12.5–23.5	0.0033 ± 0.0006	229.5 ± 6.5
12.5–23.5, 33.5–43.5	0.0048 ± 0.0004	218.4 ± 9.4

[Eq. (2a)] which, as it was already explained, corresponds to a smooth transition from representation (2b) to the expansion (2c) of the scaling function $f(x)$. For $m = 0$, $T \leqslant T_c$, the coexistence curve has a normal scaling behavior near the critical point, $|\rho_B(0)| \sim |t|^\beta$, and for $B = 3.6/(\pi r_0^2 \langle\tau\rangle)$ a good description of the peripheral freeze-out states in class (a) is obtained along this curve. In general, the lines of constant m in Fig. 4 provide us with guidance for the identification of the experimental freeze-out states as critical states. In fact, the cluster of experimental points in the area $|m| \leqslant 0.09$, corresponding to a domain in chemical potential $210 \leqslant \mu_B \leqslant 250$ MeV, is an example of freeze-out systems consistent with the critical equation of state. However, the freeze-out system at RHIC (Au + Au, $\sqrt{s} \simeq 130$ GeV) violates strongly the critical equation of state and therefore a drastic change of the collision parameters is needed (lower energy, smaller systems) to capture freeze-out states consistent with criticality [22].

In conclusion, we have shown that the universal form of the critical equation of state for systems belonging to the 3D Ising universality class [6] can be fully exploited in experiments with nuclei to identify critical QCD states at the freeze-out regime. In this approach, and in accordance with the universality principle, we have replaced in the scaling function of the Ising model (critical equation of state) the order parameter, the reduced temperature, and the external field (H) with the net-baryon density n_B, the reduced freeze-out temperature (t), and the chemical potential (m), respectively. This choice avoids the general construction discussed recently [23] in which a linear combination of the reduced temperature and chemical potential appears in the replacement described earlier in this article. Because the exact solution of the QCD critical line is not yet known, this ambiguity can be removed

only with the help of measurements. In fact, assuming that the critical line (coexistence curve) in the phase diagram (n_B, T) of strongly interacting matter follows closely the freeze-out curve in the same diagram, existing measurements (especially at the SPS) suggest that the freeze-out states near the critical point are well described by the Ising critical line as shown in Fig. 4 (coexistence curve: $m = 0$, $T \leqslant T_c$). This remark justifies *a posteriori* the choice of the conventional replacement $(t, \frac{H}{H_c}) \rightarrow (t, m)$ in our treatment, which leads to the critical equation of state (1b).

Finally, with the help of Eq. (1b) we have found that existing measurements of n_B, T, μ_B at SPS energies, reveal, within experimental error, a class of freeze-out states belonging to the critical isotherm of the QCD universality class and leading, as a consequence, to a divergent baryon-number susceptibility. This phenomenon is a strong indication for the existence of a QCD critical point in the neighborhood of these states ($\mu_{B,c} \simeq 222$ MeV, $T_c \simeq 155$ MeV). The overall analysis suggests that new, high-precision measurements in experiments with light nuclei (S + S, Si + Si, C + C) are needed (SPS-NA61, RHIC at low energies) to discover the exact location of the QCD critical point in the phase diagram [22,24].

This work was financially supported by the Research Committee of the University of Athens (research funding program Kapodistrias).

[1] M. A. Stephanov, Prog. Theor. Phys. Suppl. **153**, 139 (2004).
[2] N. G. Antoniou, F. K. Diakonos, A. S. Kapoyannis, and K. S. Kousouris, Phys. Rev. Lett. **97**, 032002 (2006).
[3] N. G. Antoniou, Y. F. Contoyiannis, F. K. Diakonos, A. I. Karanikas, and C. N. Ktorides, Nucl. Phys. **A693**, 799 (2001).
[4] R. Casalbuoni, PoS CPOD2006:001 (2006).
[5] H. Meyer-Ortmans, Rev. Mod. Phys. **68**, 473 (1996).
[6] Denjoe O' Connor, J. A. Santiago, and C. R. Stephens, J. Phys. A: Math. Theor. **40**, 901 (2007).
[7] H. Appelshäuser *et al.* (NA49 Collaboration), Phys. Rev. Lett. **82**, 2471 (1999).
[8] G. E. Cooper (NA49 Collaboration), Nucl. Phys. **A661**, 362c (1999).
[9] T. Alber *et al.* (NA35 Collaboration), Eur. Phys. J. C **2**, 643 (1998).
[10] D. Rohrich (NA35 Collaboration), Nucl. Phys. **A566**, 35c (1994).
[11] F. Becattini, M. Gazdzicki, and J. Sollfrank, Eur. Phys. J. C **5**, 143 (1998).
[12] P. Braun-Munzinger, J. Stachel, J. P. Wessels, and N. Xu, Phys. Lett. **B365**, 1 (1996).
[13] Latest NA49 results: na49compil.pdf and references therein (http://na49info.web.cern.ch/na49info/na49/Archives/Data/Na49NumericalResults).
[14] F. Becattini, J. Manninen, and M. Gazdzicki, Phys. Rev. C **73**, 044905 (2006).
[15] F. Becattini, L. Maiani, F. Piccinini, A. D. Polosa, and V. Riquer, Phys. Lett. **B632**, 233 (2006).
[16] C. Adler *et al.* (STAR Collaboration), Phys. Rev. Lett. **89**, 202301 (2002).
[17] John Adams *et al.* (STAR Collaboration), Phys. Rev. C **70**, 041901 (2004).
[18] C. Adler *et al.* (STAR Collaboration), Phys. Rev. Lett. **89**, 092301 (2002).
[19] B. B. Back *et al.*, PHOBOS White Paper on discoveries at RHIC, Nucl. Phys. **A757**, 28 (2005).
[20] P. Braun-Munzinger, K. Redlich, and J. Stachel, in *Quark Gluon Plasma 3*, edited by R. C. Hwa and Xin-Nian Wang (World Scientific Publishing, Singapore, 2004), p. 491.
[21] A. S. Kapoyannis, Eur. Phys. J. C **51**, 135 (2007); **51**, 1013 (2007).
[22] Can We Discover the QCD Critical Point at RHIC?, in *Proceedings of RIKEN BNL Research Center Workshop*, BNL-75692-2006.
[23] K. Rummukainen, M. Tsypin, K. Kajantie, M. Laine, and M. E. Shaposhnikov, Nucl. Phys. **B532**, 283 (1998); M. A. Stephanov, K. Rajagopal, and E. V. Shuryak, Phys. Rev. Lett. **81**, 4816 (1998); F. Karsch, D. Kharzeev, and K. Tuchin, Phys. Lett. **B663**, 217 (2008); C. Sasaki and K. Redlich, Phys. Rev. C **79**, 055207 (2009).
[24] N. G. Antoniou *et al.* (NA61 Collaboration), CERN-SPSC-P-330.